Controllable circular Airy beams via dynamic linear potential

Hua Zhong[1], Yiqi Zhang[1],* Milivoj R. Belić[2], Changbiao Li[1], Feng Wen[1], Zhaoyang Zhang[1], and Yanpeng Zhang[1]
[1]*Key Laboratory for Physical Electronics and Devices of the Ministry of Education & Shaanxi Key Lab of Information Photonic Technique, Xi'an Jiaotong University, Xi'an 710049, China*
[2]*Science Program, Texas A&M University at Qatar, P.O. Box 23874 Doha, Qatar*
(Dated: March 29, 2016)

We investigate controllable spatial modulation of circular autofocusing Airy beams, under action of different dynamic linear potentials, both theoretically and numerically. We introduce a novel treatment method in which the circular Airy beam is represented as a superposition of narrow azimuthally-modulated one-dimensional Airy beams that can be analytically treated. The dynamic linear potentials are appropriately designed, so that the autofocusing effect can either be weakened or even eliminated when the linear potential exerts a "pulling" effect on the beam, or if the linear potential exerts a "pushing" effect, the autofocusing effect can be greatly strengthened. Numerical simulations agree with the theoretical results very well.

Keywords: autofocusing, linear potential

arXiv:1603.08349v1 [physics.optics] 28 Mar 2016

* zhangyiqi@mail.xjtu.edu.cn

I. INTRODUCTION

In quantum mechanics, the Airy function has been shown to be a solution of the potential-free Schrödinger equation [1]. Since the Airy wave function is not a realistic physical quantity, due to its infinite energy, the investigation of Airy wavepackets in physics did not attract much attention until the introduction of finite-energy Airy beams in optics [2, 3]. Such beams possess interesting and useful self-accelerating, self-healing [4] and nondiffracting properties. Hence, in the past decade topics related with Airy beams received intense attention. Thus far, investigations of Airy beams have been reported in nonlinear media [5–11], Bose-Einstein condensates [12], on the surface of a metal [13–16], optical fibers [17–20], and other systems. To manipulate the propagation of Airy beams, external potentials such as harmonic [21–23] or a linear potenial [24, 25], have been introduced. For more details, the reader may consult review articles [26–28] and references therein.

On the other hand, in more than one dimension the circular Airy (CAi) beams, as radially symmetric beams that possess autofocusing property [29–32], have stirred wide interest in the past few years. It has been demonstrated that CAi beams can be used to trap and guide microparticles [33, 34] and even to produce the so-called bottle beams [35] and light bullets [36]. Similar to the finite-energy Airy beams, CAi beams can also be controlled and manipulated by potentials [37–39]. Recent research has shown that the propagation trajectory as well as the position of autofocusing points of the CAi beam can be controlled by a dynamic linear potential [37]. However, for fuller understanding further investigation of CAi beams is required. Interesting questions remain unanswered. Can the layers of CAi beams be modulated during propagation? Can the autofocusing effect be weakened or maybe strengthened? We answer these questions in this article.

Here, we introduce specific linear potentials and investigate the corresponding influence on the propagation of CAi beams. Since the linear potential is similar to a "force" in the classical mechanics [1], it will pull or push the CAi beams during propagation. We give an analytical solution for a two-dimensional CAi beam propagating in the linear potential by an analogy to that for a one-dimensional finite-energy Airy beam, and then carry out numerical simulations to verify its validity. We find that the autofocusing can be strengthened when the linear potential plays a "pushing" role, while when it plays a "pulling" role, the autofocusing effect can be weakened or even eliminated.

The setup of the article is as follows. In Sec. II, we introduce the theoretical model, and in Sec. III, we present our theoretical and numerical results for different linear potentials. In Sec. IV, different from Sec. III where an exponential apodization is adopted, we briefly discuss the case with a Gaussian apodization. We conclude the paper and display some extended discussions in Sec. V.

II. THEORETICAL MODEL

The propagation dynamics of the CAi beam is described by the following Schrödinger equation:

$$i\frac{d\psi}{dz}+\frac{1}{2}\left(\frac{\partial^2\psi}{\partial x^2}+\frac{\partial^2\psi}{\partial y^2}\right)-V(x,y,z)\psi=0, \tag{1}$$

where ψ is the beam envelope, x and y are the normalized transverse coordinates, and z is the propagation distance, scaled by some characteristic transverse width x_0 and the corresponding Rayleigh length kx_0^2, respectively. Here, $k=2\pi n/\lambda_0$ is the wavenumber, n the index of refraction, and λ_0 the wavelength in free space. For our purposes, the values of parameters can be taken as $x_0=100\,\mu$m, and $\lambda_0=600\,$nm. The external potential is chosen in a specific form $V(x,y,z)=d(z)r/2$, where $r=\sqrt{x^2+y^2}$. Thus, it is linear in r, with the scaling factor d depending on the longitudinal coordinate. In this form, it is known as the *dynamical* linear potential [25, 37, 38]. In polar coordinates, Eq. (1) can be rewritten as

$$i\frac{d\psi}{dz}+\frac{1}{2}\left(\frac{\partial^2\psi}{\partial r^2}+\frac{1}{r}\frac{\partial\psi}{\partial r}\right)-\frac{d(z)}{2}r\psi=0. \tag{2}$$

In the (1+1)-dimensional limit, Eq. (1) can be written as

$$i\frac{\partial\psi}{\partial z}+\frac{1}{2}\frac{\partial^2\psi}{\partial x^2}-\frac{d(z)}{2}|x|\psi=0, \tag{3}$$

which clearly is a linear potential. Without the absolute value sign on x, Eq. (3) is the same as that treated in [25]. However, with the absolute value, one can manage this problem for $x>0$ and $x<0$ separately [40]. In Eq. (1) or Eq. (2), we assume that the input beam is an inward CAi beam

$$\psi(x,y)=\mathrm{Ai}(r_0-r)\exp[a(r_0-r)], \tag{4}$$

where a is the decay parameter – a positive real number that makes the total energy finite, and r_0 is the initial radius of the main Airy ring. For our purpose, we assume $r_0 = 5$; the corresponding intensity distribution of the input is shown in Fig. 1(a). We note that it is hard to find an analytical solution of Eq. (1) or Eq. (2) by the method developed in [25], because of the difficulty with the Fourier transform of the last term in Eq. (1) or the zero-order Hankel transform of the last term in Eq. (2). Here, we develop an approximate but accurate method to solve this problem – by introducing an azimuthal modulation of the CAi beam in Eq. (4),

$$\psi_{\rm az}(x,y) = {\rm Ai}(r_0 - r)\exp[a(r_0 - r)]\exp\left(-\frac{(\theta-\theta_0)^2}{w_0^2}\right), \tag{5}$$

with w_0 being the width of the modulation, $\theta = \arctan(y/x)$ being the azimuthal angle, and θ_0 indicating the modulation direction.

In Fig. 1, we depict some input possibilities. First, we set $w_0 = 1.5$ and $\theta_0 = 0$; the corresponding intensity is displayed in Fig. 1(b), which is a crescent-like structure with many layers. Clearly, the appearance of this structure is due to the azimuthal modulation. If the value of w_0 is small enough, the azimuthal modulation will results in a very narrow structure, which is quite similar to a one-dimensional finite-energy Airy beam (viz. $w_0 \to 0$). In fact, one can use Dirac's delta fuction

$$\delta(\theta-\theta_0) = \lim_{w_0\to 0}\exp\left(-\frac{(\theta-\theta_0)^2}{w_0^2}\right) = \begin{cases} 1, & \theta = \theta_0 \\ 0, & \theta \neq \theta_0 \end{cases}$$

to transform the CAi beam in Eq. (5) into the one-dimensional finite-energy Airy beam.

In Fig. 1(c), we show such a structure by choosing $w_0 = 0.05$ and $\theta_0 = 0$. For the azimuthal modulation along other azimuthal angles, one can rotate the transverse axes and obtain the same case as for $\theta_0 = 0$, by using the rotation matrix

$$\begin{bmatrix} x_p \\ y_p \end{bmatrix} = \begin{bmatrix} \cos\theta_0 & -\sin\theta_0 \\ \sin\theta_0 & \cos\theta_0 \end{bmatrix}\begin{bmatrix} x \\ y \end{bmatrix},$$

where x_p and y_p are the coordinates after rotation. One can verify that the positive x direction after rotation is overlapping with the azimuthal modulation along θ_0, because

$$\tan\theta_p = \frac{y_p}{x_p} = \frac{x\sin\theta_0 + y\cos\theta_0}{x\cos\theta_0 - y\sin\theta_0} = \tan(\theta+\theta_0).$$

As a result, the CAi beam can be approximately viewed as an assembly of one-dimensional finite-energy Airy beams associated with the transformed coordinate x_p (which is the variable of the transformed Airy beam), of the form

$$\psi(x,y) = \sum_{\theta_0=-\pi}^{+\pi} {\rm Ai}(r_0 - x_p)\exp[a(r_0 - x_p)]. \tag{6}$$

In Fig. 1(d), we choose 40 azimuthally modulated CAi beams along different angles, to mimic the initial CAi beam shown in Fig. 1(a). One can see that such an approximation makes sense.

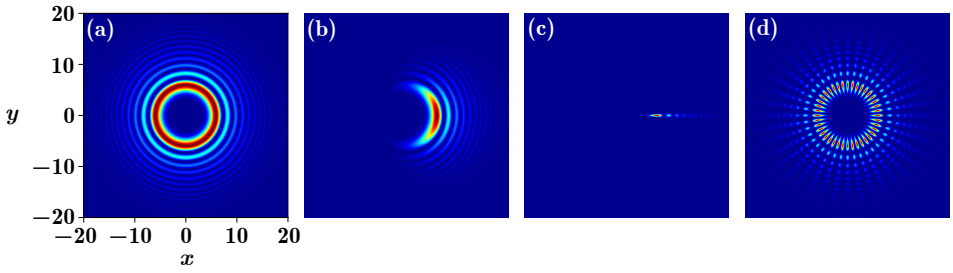

FIG. 1. Input beam intensities. (a) An example of finite-energy circular Airy beam. (b) An azimuthally-modulated circular Airy beam, with $w_0 = 1.5$. (c) Same as (b), but with $w_0 = 0.05$. (d) A combination of 40 azimuthally modulated circular Airy beams along different azimuthal directions, according to Eq. (6). Other parameters: $r_0 = 5$ and $a = 0.1$. All the panels share the same variables and dimensions.

Therefore, the description of the propagation of a CAi beam can be approximately reduced to the one-dimensional case [41], i.e., to Eq. (3), which is a much simpler problem. Thus, the propagation of the CAi beam can be described by

$$\begin{aligned}\psi(x,y,z) = C\sum_{\theta_0=-\pi}^{+\pi} \mathrm{Ai}\left[iaz + \left(\frac{1}{2}f_1 - \frac{1}{4}z^2 + (r_0 - x_p)\right)\right] \times \\ \exp\left[a\left(\frac{1}{2}f_1 - \frac{1}{2}z^2 + (r_0 - x_p)\right)\right] \times \\ \exp\left[i\left(\frac{1}{2}a^2 z + \frac{1}{4}zf_1 - \frac{1}{8}f_2 - \frac{1}{12}z^3 - \frac{1}{2}(r_0 - x_p)g + \frac{1}{2}(r_0 - x_p)z\right)\right],\end{aligned} \tag{7}$$

by analogy to the one-dimensional case [25]. In Eq. (7),

$$g(z) = \int_0^z d(t)dt,$$

$$f_1(z) = f_0 + \int_0^z g(t)dt,$$

and

$$f_2(z) = \int_0^z g^2(t)dt,$$

where f_0 is a constant that guarantees $f_1(z = 0) = 0$. In addition, parameter C in Eq. (7) is a normalization parameter, which makes a balance between the total intensity of components and the intensity of the CAi beam. According to Eq. (7), the trajectory of each component in a dynamic linear potential is

$$x_p = r_0 + \frac{1}{2}f_1 - \frac{1}{4}z^2, \tag{8}$$

which is related to the type of the potential. In other words, the CAi beam can be effectively manipulated by the linear potential. It is clear that the accuracy of our approximation improves as the summation in Eq. (7) is performed over more terms. We stress the fact that the solution in Eq. (7) can be viewed as a superposition of infinitely many one-dimensional Airy beams from different directions, which is an extension of the work done in [9]. In addition, we also have to mention that the summation in Eq. (7) and the trajectory in Eq. (8) are somewhat rude approximations, because we omitted the absolute value sign in Eq. (3) in the analysis, so that the results for components displayed in Eqs. (7) and (8) will not be very accurate in case of collisions during propagation. However, such inaccuracy will be waived if the components do not collide with each other.

If $d(z) \equiv 0$, Eq. (1) reduces to the Schrödinger equation in free space and the propagation of CAi beam according to such a model has already been reported [29]. Equation (7) can describe the autofocusing effect effectively. As a test, one can choose only two components with $\theta_0 = 0$ and π to mimic the autofocusing effect, which is similar to Fig. 2 in [9]. If there is no autofocusing during propagation, Eq. (7) can be rewritten as

$$\begin{aligned}\psi(x,y,z) = &\mathrm{Ai}\left[iaz + \left(\frac{1}{2}f_1 - \frac{1}{4}z^2 + (r_0 - r)\right)\right] \times \\ &\exp\left[a\left(\frac{1}{2}f_1 - \frac{1}{2}z^2 + (r_0 - r)\right)\right] \times \\ &\exp\left[i\left(\frac{1}{2}a^2 z + \frac{1}{4}zf_1 - \frac{1}{8}f_2 - \frac{1}{12}z^3 - \frac{1}{2}(r_0 - r)g + \frac{1}{2}(r_0 - r)z\right)\right],\end{aligned} \tag{9}$$

which is invalid when "autofocusing" happens. For accuracy, the focusing is now guided by the linear potential, and it is not an automatic behavior; that's why here (and from now on) we place the quotation marks on the word. But, to stress, autofocusing is adequately described by Eq. (7).

In summary, our analysis is based on applying the azimuthal modulation to CAi beams; this novel treatment helps one reduce the two-dimensional problem into a simpler one-dimensional case. Using Eqs. (7) and (9), the propagation of a CAi beam manipulated by a dynamic linear potential can now be simply described. In the following, we investigate the influence of different potentials on Airy beams during propagation.

III. RESULTS AND DISCUSSIONS

A. The case $d(z) = 1$

According to Eq. (8), the trajectory of each component is

$$x_p = r_0, \tag{10}$$

which is independent on the propagation distance, i.e., the size of the ring of the CAi beam will not change during propagation. Actually, Eq. (3) with $d(z) = 1$ has already been solved in [24], in which the trajectory of the one-dimensional finite-energy Airy beam is a straight line. Since the beam will not focus during propagation, Eq. (9) can be used to describe the propagation.

The result is displayed in Fig. 2, in which Fig. 2(a) is the analytical result according to Eq. (9), and Fig. 2(b) is the corresponding numerical simulation of Eq. (1). Due to rotational symmetry of the CAi beam, we only exhibit the transverse intensity distribution along the x axis ($y = 0$) during propagation. One can see that the analytical and numerical results agree with each other very well. To elucidate propagation, we also present beam intensities obtained numerically at certain distances, as displayed in Figs. 2(c1)-2(c3). Indeed, the size of the ring of the CAi beam remains the same during propagation, but the intensity dims. For this case, the linear potential exerts a "pulling" influence that can balance the virtual force which makes the beam focus.

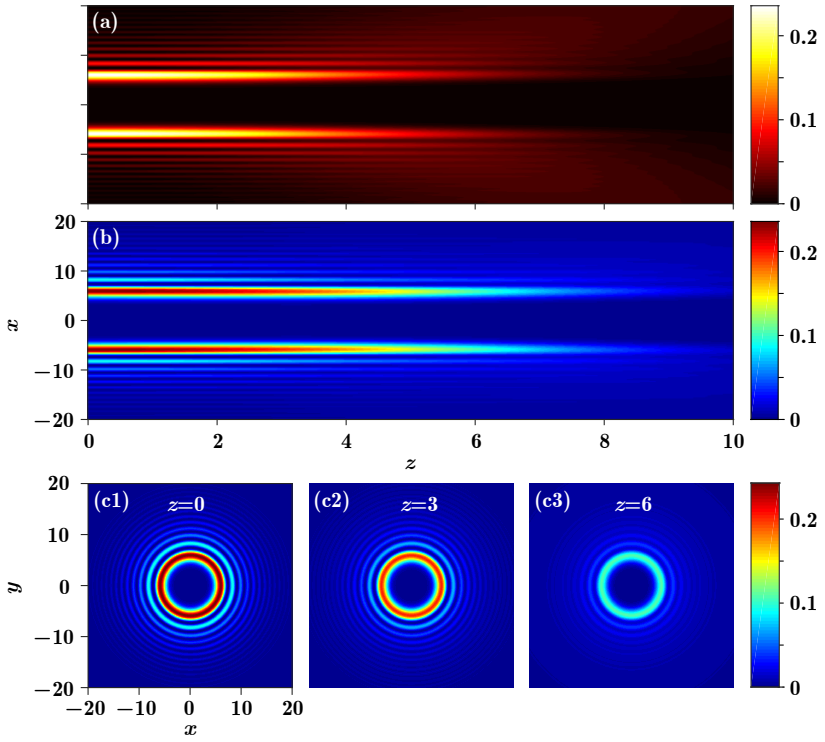

FIG. 2. (a) Analytical intensity distribution of a CAi beam during propagation in the $x-z$ plane at $y = 0$, according to Eq. (9), for $d = 1$. (b) Same as (a), but for numerical simulation. (c) Intensity profiles of CAi beam at different propagation distances (noted in each panel). Other parameters: $r_0 = 5$ and $a = 0.1$. All the panels in (c) share the same variables, dimensions, and color scales.

B. The case $d(z) = 1 + 4\pi^2 \cos(\pi z)$

For this case, the trajectory of each component can be written as

$$x_p = r_0 - 2\cos(\pi z) + 2, \tag{11}$$

which is same as the one displayed in [25] with the period of 2, and the trajectory of the one-dimensional finite-energy Airy beam does not move across $x_p = 0$. So, there will be no "autofocusing" of the CAi beam, which means that the

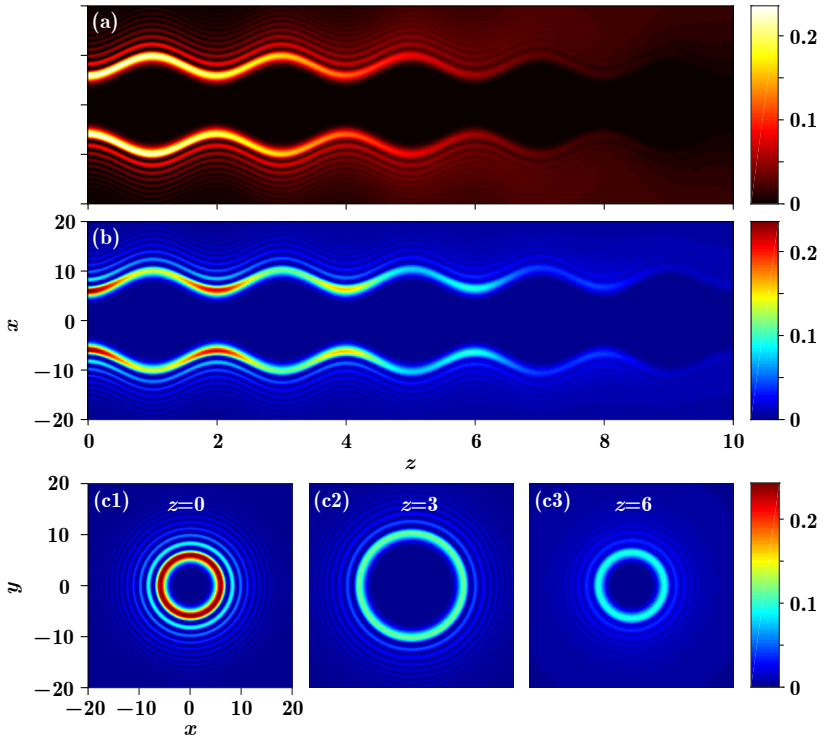

FIG. 3. Same as Fig. 2, but for $d(z) = 1 + 4\pi^2 \cos(\pi z)$.

linear potential also exerts a "pulling" effect. As a result, the propagation for this case can still be described by Eq. (9). The corresponding result is exhibited in Fig. 3, the setup of which is the same as that of Fig. 2. Again, the analytical and numerical results agree with each other very well.

C. The case $d(z) = 13 - 12z$

According to Eq. (8), the trajectory for this case is

$$x_p = r_0 - z^3 + 3z^2, \tag{12}$$

which indicates that the CAi beam will undergo "autofocusing" during propagation, so that the description of the propagation should be based on Eq. (7). In Fig. 4(a), the maximum of intensity during propagation is exhibited. In order to make a comparison, we take the same values for a as used in [29] and the same normalized intensity of the input. One can clearly see that the beam intensity decreases initially, but then increases to almost 500 after "autofocusing", which is much higher than that without a potential. Undoubtedly, the potential exerts a strong "pushing" effect that strengthens the focusing.

To show the "pushing" effect more clearly, we display the propagation of the components corresponding to $\theta_0 = 0$ and $\theta_0 = \pi$ in the inset in Fig. 4(a). It is evident that at first the two components tend to separate before the focusing point, but then they converge. The slope of the components at the colliding point is bigger than that without a potential, as in [29], which can be viewed that the components acquire a larger speed because of the "pushing" effect; hence, the "autofocusing" is strengthened. However, according to the propagation in the inset, one may doubt the accuracy of our analysis, because the intensity at the "autofocusing" point is not the largest. The explanation is that one cannot use only two one-dimensional Airy beams to obtain the real physical picture of the propagation of the full CAi beam – such an approximation is too poor. If another pair of components is added, the intensity at and only at the "autofocusing" point will be larger, due to the collision of four components. The intensity at the "autofocusing" point will reach an enormous value when numerous pairs of components are considered simultaneously; such a consideration can approximate the propagation of the CAi beam very well. Since the theoretical trajectories in Eq. (8) do not consider the absolute value sign in Eq. (3), the theoretical trajectories are only valid before collision occurs.

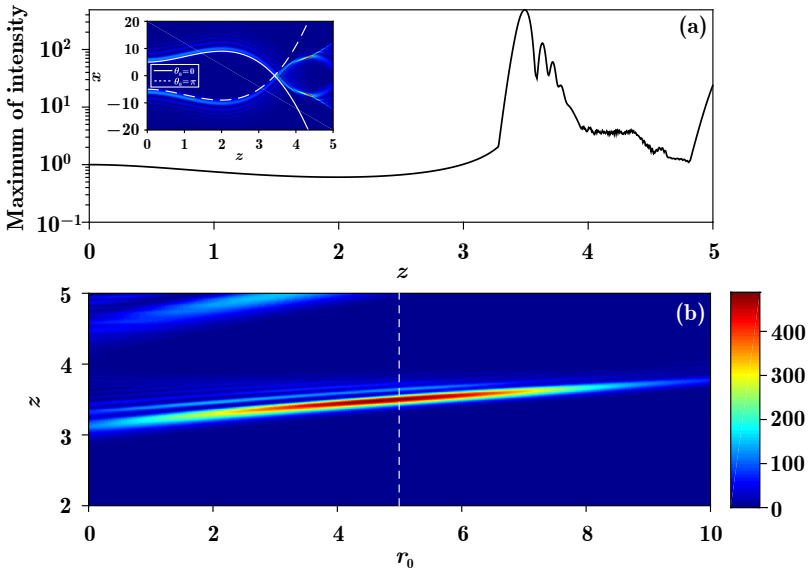

FIG. 4. (a) Maximum of the beam intensity during propagation for $d(z) = 13 - 12z$ and $r_0 = 5$. The maximum of the beam intensity at $z = 0$ is 1. Inset shows the propagation of the components corresponding to $\theta_0 = 0$ and $\theta_0 = \pi$, and the corresponding theoretical trajectories. (b) The maximum of the beam intensity as a function of r_0 and z. The white dashed line corresponds to the curve in (a). The decay parameter is $a = 0.05$.

Similar to the previous study [29], r_0 also affects the maximum of the beam intensity (MBI) reached during propagation. To observe such a dependence more clearly, we show the change of the MBI as a function of both r_0 and the propagation distance, as displayed in Fig. 4(b). One sees that the MBI first increases and then decreases with the increasing of r_0, and the MBI reaches a maximum around $r_0 = 5$. In addition, one can also see that the location of MBI also changes with r_0. The reason is that the "autofocusing" effect requires a longer distance to establish itself when r_0 increases.

D. The case $d(z) = 1 - 4H(z-2)/\left[(z-4)z+5\right]^{3/2}$

The function $H(z-2)$ here is the Heaviside step function, which demands

$$H(z-2) = \begin{cases} 0, & \text{for } (z \le 2), \\ 1, & \text{for } (z > 2). \end{cases}$$

Therefore, the trajectory for this case can be written as

$$x_p = \begin{cases} r_0, & \text{for } (z \le 2), \\ r_0 + 2 - 2\sqrt{(z-4)z+5}, & \text{for } (z > 2). \end{cases} \tag{13}$$

Similar to the case in Sec. III C, the beam will "autofocus" during propagation, and we display the MBI for this case in Fig. 5. In Fig. 5(a), one finds that the MBI during propagation is about 60 times of the input. This value is much lower than that in [29], as well as of that in Sec. III C. From the inset in Fig. 5(a), one finds the reason easily – the speed (slope) at the colliding point is smaller than that in [29], because of the "pulling" effect. Figure 5(b) shows the MBI as a function of r_0 and z, from which one can see that the peak of the MBI is still no more than 65, so the linear potential in this case exerts a "pulling" influence, which weakens the autofocusing effect.

IV. CIRCULAR AIRY BEAM WITH GAUSSIAN APODIZATION

By using a Gaussian apodization, the CAi beam can also be made finite-energy, of the form

$$\psi = \mathrm{Ai}(r_0 - r)\exp\left(-\frac{(r_0 - r)^2}{w^2}\right),$$

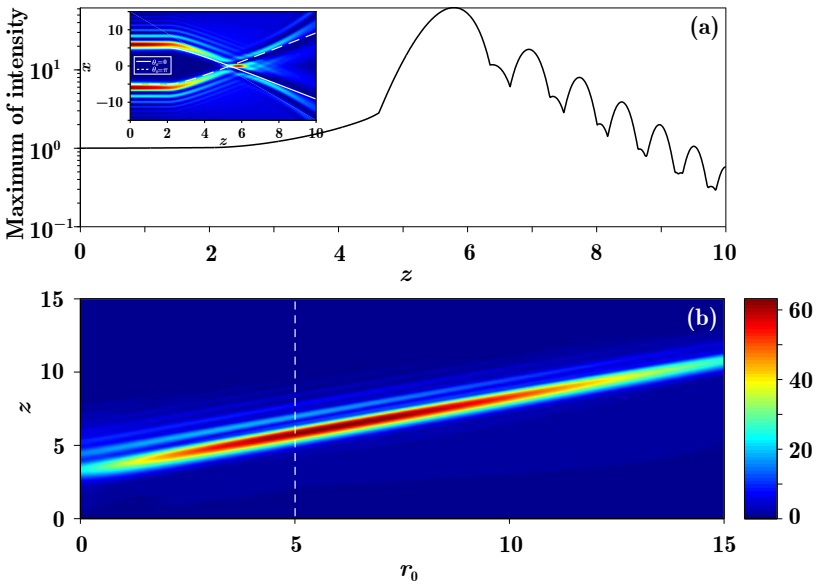

FIG. 5. Figure setup is as in Fig. 4.

where w is related to the beam width of the Gaussian apodization. Following the same procedure as before, the solution can be written as

$$\psi(x,y,z) = \frac{1}{\sqrt{\sigma}} \sum_{\theta_0=-\pi}^{+\pi} \mathrm{Ai}\left[\frac{1}{\sigma}\left((r_0 - x_p) + \frac{f_1}{2}\right) - \frac{z^2}{4\sigma^2}\right] \exp\left[\frac{-1}{\sigma w^2}\left((r_0 - x_p) + \frac{f_1}{2}\right)\right] \times \exp\left\{i\left[-\frac{f_2}{8} - \frac{D}{2}(r_0 - x_p) + \frac{z}{2\sigma^2}\left(r_0 - x_p + \frac{f_1}{2} - \frac{z^2}{6\sigma}\right)\right]\right\}, \tag{14}$$

where $\sigma = 1 + 2iz/w^2$. If there is no "autofocusing" during propagation, the solution in Eq. (14) can be directly rewritten as

$$\psi(x,y,z) = \frac{1}{\sqrt{\sigma}} \mathrm{Ai}\left[\frac{1}{\sigma}\left((r_0 - r) + \frac{f_1}{2}\right) - \frac{z^2}{4\sigma^2}\right] \exp\left[\frac{-1}{\sigma w^2}\left((r_0 - r) + \frac{f_1}{2}\right)\right] \times \exp\left\{i\left[-\frac{f_2}{8} - \frac{D}{2}(r_0 - r) + \frac{z}{2\sigma^2}\left(r_0 - r + \frac{f_1}{2} - \frac{z^2}{6\sigma}\right)\right]\right\}. \tag{15}$$

Clearly, the trajectory of each component can be written as

$$x_p = r_0 - \frac{z^2 w^4}{4(w^4 + 4z^2)} + \frac{f_1}{2}, \tag{16}$$

which is not only related to the linear potential, but also to the beam width of the Gaussian apodization. If the condition $w^2 \gg z$ is fulfilled (this condition can be relatively easily fulfilled when the propagation distance is not too long), Eq. (16) will be reduced to Eq. (8); therefore, all the phenomena obtained in Sec. III can also be realized for Gaussian apodization. In other words, the Gaussian-apodized CAi beams can also be well controlled and manipulated. However, one needs to bear in mind that such an apodization introduces another degree of freedom in the beam manipulation.

As an elucidation, in Fig. 6 we display the numerical simulations of a CAi beam with Gaussian apodization in a dynamic linear potential that is used in Sec. III A; the dashed curves show the corresponding analytical trajectories. One can find that, in comparison with the trajectory in Fig. 6(b), the trajectory in Fig. 6(a) is much more similar to that in Fig. 2(b), because the value of w in the latter case is bigger, which guarantees the validity of the condition $w^2 \gg z$ over a longer propagation distance.

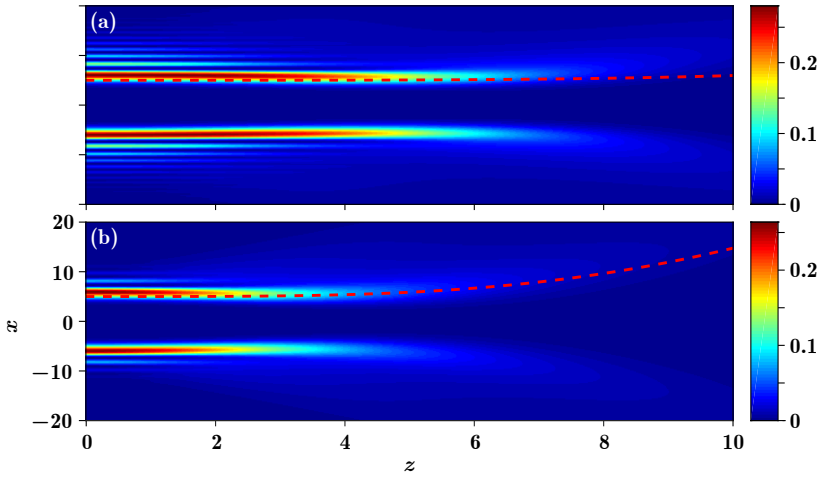

FIG. 6. Same as Fig. 2(b), but for Gaussian apodization with (a) $w = 10$, and (b) $w = 5$. The dashed curves represent the analytical trajectories. The panels share the same variables and dimensions.

V. CONCLUSION

In summary, we have theoretically and numerically investigated the spatial guidance of CAi beams, by using different types of dynamic linear potentials. We find that the accelerating trajectory of the CAi beam can be controlled by the linear potential effectively. Such a manipulation may weaken (even eliminate) or strengthen the autofocusing effect of the CAi beam, depending on the form of the linear potential. Our results broaden the potential applications of CAi beams in trapping and manipulating microparticles, offering potential use in optics, biology, and other disciplines.

Last but not least, we would like to point out that the analysis presented here can also be applied to the outward CAi beams [42], but the validity is more limited, because the outward CAi beams always produce a focusing peak at the beam's center, which is not the case for the inward CAi beams if the linear potential is well chosen. As reported in [37], the manipulation on the "autofocusing" effect can be enriched if one launches the input beam appropriately (e.g., the incident angle), which is independent of the potential.

ACKNOWLEDGMENT

This work was supported by the 973 Program (2012CB921804), KSTIT of Shaanxi province (2014KCT-10), NSFC (11474228, 61308015), and the NPRP 6-021-1-005 project of the Qatar National Research Fund (a member of the Qatar Foundation). MRB also acknowledges support by the Al Sraiya Holding Group.

[1] M. V. Berry and N. L. Balazs, *Nonspreading wave packets*, Am. J. Phys. **47**, 264 (1979).
[2] G. A. Siviloglou and D. N. Christodoulides, *Accelerating finite energy Airy beams*, Opt. Lett. **32**, 979 (2007).
[3] G. Siviloglou, J. Broky, A. Dogariu, and D. Christodoulides, *Observation of Accelerating Airy Beams*, Phys. Rev. Lett. **99**, 213901 (2007).
[4] J. Broky, G. A. Siviloglou, A. Dogariu, and D. N. Christodoulides, *Self-healing properties of optical Airy beams*, Opt. Express **16**, 12880 (2008).
[5] I. Kaminer, M. Segev, and D. N. Christodoulides, *Self-Accelerating Self-Trapped Optical Beams*, Phys. Rev. Lett. **106**, 213903 (2011).
[6] A. Lotti, D. Faccio, A. Couairon, D. G. Papazoglou, P. Panagiotopoulos, D. Abdollahpour, and S. Tzortzakis, *Stationary nonlinear Airy beams*, Phys. Rev. A **84**, 021807 (2011).
[7] I. Dolev, I. Kaminer, A. Shapira, M. Segev, and A. Arie, *Experimental Observation of Self-Accelerating Beams in Quadratic Nonlinear Media*, Phys. Rev. Lett. **108**, 113903 (2012).
[8] Y. Q. Zhang, M. Belić, Z. K. Wu, H. B. Zheng, K. Q. Lu, Y. Y. Li, and Y. P. Zhang, *Soliton pair generation in the interactions of Airy and nonlinear accelerating beams*, Opt. Lett. **38**, 4585 (2013).
[9] Y. Q. Zhang, M. R. Belić, H. B. Zheng, H. X. Chen, C. B. Li, Y. Y. Li, and Y. P. Zhang, *Interactions of Airy beams, nonlinear accelerating beams, and induced solitons in Kerr and saturable nonlinear media*, Opt. Express **22**, 7160 (2014).

[10] M. Shen, J. Gao, and L. Ge, *Solitons shedding from Airy beams and bound states of breathing Airy solitons in nonlocal nonlinear media*, Sci. Rep. **5**, 9814 (2015).

[11] F. Diebel, B. M. Bokić, D. V. Timotijević, D. M. J. Savić, and C. Denz, *Soliton formation by decelerating interacting Airy beams*, Opt. Express **23**, 24351 (2015).

[12] N. K. Efremidis, V. Paltoglou, and W. von Klitzing, *Accelerating and abruptly autofocusing matter waves*, Phys. Rev. A **87**, 043637 (2013).

[13] A. Salandrino and D. N. Christodoulides, *Airy plasmon: a nondiffracting surface wave*, Opt. Lett. **35**, 2082 (2010).

[14] P. Zhang, S. Wang, Y. Liu, X. Yin, C. Lu, Z. Chen, and X. Zhang, *Plasmonic Airy beams with dynamically controlled trajectories*, Opt. Lett. **36**, 3191 (2011).

[15] A. Minovich, A. E. Klein, N. Janunts, T. Pertsch, D. N. Neshev, and Y. S. Kivshar, *Generation and Near-Field Imaging of Airy Surface Plasmons*, Phys. Rev. Lett. **107**, 116802 (2011).

[16] L. Li, T. Li, S. M. Wang, C. Zhang, and S. N. Zhu, *Plasmonic Airy Beam Generated by In-Plane Diffraction*, Phys. Rev. Lett. **107**, 126804 (2011).

[17] Y. Hu, M. Li, D. Bongiovanni, M. Clerici, J. Yao, Z. Chen, J. Azaña, and R. Morandotti, *Spectrum to distance mapping via nonlinear Airy pulses*, Opt. Lett. **38**, 380 (2013).

[18] R. Driben, Y. Hu, Z. Chen, B. A. Malomed, and R. Morandotti, *Inversion and tight focusing of Airy pulses under the action of third-order dispersion*, Opt. Lett. **38**, 2499 (2013).

[19] L. Zhang, K. Liu, H. Zhong, J. Zhang, Y. Li, and D. Fan, *Effect of initial frequency chirp on Airy pulse propagation in an optical fiber*, Opt. Express **23**, 2566 (2015).

[20] Y. Hu, A. Tehranchi, S. Wabnitz, R. Kashyap, Z. Chen, and R. Morandotti, *Improved Intrapulse Raman Scattering Control via Asymmetric Airy Pulses*, Phys. Rev. Lett. **114**, 073901 (2015).

[21] M. A. Bandres and J. C. Gutiérrez-Vega, *Airy-Gauss beams and their transformation by paraxial optical systems*, Opt. Express **15**, 16719 (2007).

[22] Y. Q. Zhang, M. R. Belić, L. Zhang, W. P. Zhong, D. Y. Zhu, R. M. Wang, and Y. P. Zhang, *Periodic inversion and phase transition of finite energy Airy beams in a medium with parabolic potential*, Opt. Express **23**, 10467 (2015).

[23] Y. Q. Zhang, X. Liu, M. R. Belić, W. P. Zhong, M. S. Petrović, and Y. P. Zhang, *Automatic Fourier transform and self-Fourier beams due to parabolic potential*, Ann. Phys. **363**, 305 (2015).

[24] W. Liu, D. N. Neshev, I. V. Shadrivov, A. E. Miroshnichenko, and Y. S. Kivshar, *Plasmonic Airy beam manipulation in linear optical potentials*, Opt. Lett. **36**, 1164 (2011).

[25] N. K. Efremidis, *Airy trajectory engineering in dynamic linear index potentials*, Opt. Lett. **36**, 3006 (2011).

[26] Y. Hu, G. A. Siviloglou, P. Zhang, N. K. Efremidis, D. N. Christodoulides, and Z. Chen, in *Nonlinear Photonics and Novel Optical Phenomena*, Springer Series in Optical Sciences, Vol. 170, edited by Z. Chen and R. Morandotti (Springer, New York, 2012) pp. 1–46.

[27] Z. Zhang, Y. Hu, J. Y. Zhao, P. Zhang, and Z. G. Chen, *Research progress and application prospect of Airy beams*, Chin. Sci. Bull. **58**, 3513 (2013).

[28] M. A. Bandres, I. Kaminer, M. Mills, B. M. Rodriguez-Lara, E. Greenfield, M. Segev, and D. N. Christodoulides, *Accelerating Optical Beams*, Opt. Phot. News **24**, 30 (2013).

[29] N. K. Efremidis and D. N. Christodoulides, *Abruptly autofocusing waves*, Opt. Lett. **35**, 4045 (2010).

[30] D. G. Papazoglou, N. K. Efremidis, D. N. Christodoulides, and S. Tzortzakis, *Observation of abruptly autofocusing waves*, Opt. Lett. **36**, 1842 (2011).

[31] I. Chremmos, N. K. Efremidis, and D. N. Christodoulides, *Pre-engineered abruptly autofocusing beams*, Opt. Lett. **36**, 1890 (2011).

[32] R.-S. Penciu, K. G. Makris, and N. K. Efremidis, *Nonparaxial abruptly autofocusing beams*, Opt. Lett. **41**, 1042 (2016).

[33] P. Zhang, J. Prakash, Z. Zhang, M. S. Mills, N. K. Efremidis, D. N. Christodoulides, and Z. Chen, *Trapping and guiding microparticles with morphing autofocusing Airy beams*, Opt. Lett. **36**, 2883 (2011).

[34] P. Li, S. Liu, T. Peng, G. Xie, X. Gan, and J. Zhao, *Spiral autofocusing Airy beams carrying power-exponent-phase vortices*, Opt. Express **22**, 7598 (2014).

[35] I. Chremmos, P. Zhang, J. Prakash, N. K. Efremidis, D. N. Christodoulides, and Z. Chen, *Fourier-space generation of abruptly autofocusing beams and optical bottle beams*, Opt. Lett. **36**, 3675 (2011).

[36] P. Panagiotopoulos, D. G. Papazoglou, A. Couairon, and S. Tzortzakis, *Sharply autofocused ring-Airy beams transforming into non-linear intense light bullets*, Nat. Commun. **4**, 2622 (2013).

[37] C.-Y. Hwang, K. Y. Kim, and B. Lee, *Dynamic Control of Circular Airy Beams With Linear Optical Potentials*, IEEE Photon. J. **4**, 174 (2012).

[38] I. D. Chremmos, Z. Chen, D. N. Christodoulides, and N. K. Efremidis, *Abruptly autofocusing and autodefocusing optical beams with arbitrary caustics*, Phys. Rev. A **85**, 023828 (2012).

[39] Y. Q. Zhang, X. Liu, M. R. Belić, W. P. Zhong, F. Wen, and Y. P. Zhang, *Anharmonic propagation of two-dimensional beams carrying orbital angular momentum in a harmonic potential*, Opt. Lett. **40**, 3786 (2015).

[40] Y. Q. Zhang, X. Liu, M. R. Belić, W. P. Zhong, Y. P. Zhang, and M. Xiao, *Propagation Dynamics of a Light Beam in a Fractional Schrödinger Equation*, Phys. Rev. Lett. **115**, 180403 (2015).

[41] Z. Zhang, J.-J. Liu, P. Zhang, P.-G. Ni, J. Prakash, Y. Hu, D.-S. Jiang, D. N. Christodoulides, and Z.-G. Chen, *Generation of autofocusing beams with multi-Airy beams*, Acta Phys. Sin. **62**, 034209 (2013).

[42] C.-Y. Hwang, K.-Y. Kim, and B. Lee, *Bessel-like beam generation by superposing multiple Airy beams*, Opt. Express **19**, 7356 (2011).